

# Stability of sub-surface oxygen at Rh(111)

M. Veronica Ganduglia-Pirovano\*, Karsten Reuter, and Matthias Scheffler  
*Fritz-Haber-Institut der Max-Planck-Gesellschaft, Faradayweg 4-6, D-14195 Berlin, Germany*  
 (October 30, 2018)

Using density-functional theory (DFT) we investigate the incorporation of oxygen directly below the Rh(111) surface. We show that oxygen incorporation will only commence after *nearly* completion of a dense O adlayer ( $\theta_{\text{tot}} \approx 1.0$  monolayer) with O in the fcc on-surface sites. The experimentally suggested octahedral sub-surface site occupancy, inducing a site-switch of the on-surface species from fcc to hcp sites, is indeed found to be a rather low energy structure. Our results indicate that at even higher coverages oxygen incorporation is followed by oxygen agglomeration in two-dimensional sub-surface islands directly below the first metal layer. Inside these islands, the metastable hcp/octahedral (on-surface/sub-surface) site combination will undergo a barrierless displacement, introducing a stacking fault of the first metal layer with respect to the underlying substrate and leading to a stable fcc/tetrahedral site occupation. We suggest that these elementary steps, namely, oxygen incorporation, aggregation into sub-surface islands and destabilization of the metal surface may be more general and precede the formation of a surface oxide at close-packed late transition metal surfaces.

PACS numbers: 81.65.Mq, 68.43.Bc, 82.65.My

## I. INTRODUCTION

Exposing a metal surface to oxygen can result in simple adsorbate covered surfaces, O sub-surface penetration or oxide formation, depending markedly on the oxygen partial pressure, substrate temperature, the crystallographic orientation of the surface, and the time of exposure. As the chemical activity of the metal surface in these different states can vary significantly, knowledge of the interaction of oxygen with metal surfaces is critical for understanding technologically important processes like e.g. oxidation catalysis. The formation of surface oxides on metal surfaces can in this respect both be beneficial, as well as detrimental. In particular, for applications such as the CO oxidation on transition metal based catalysts, oxide formation at the catalyst's surface in the reactive environment was primarily viewed as leading to an inactive surface oxide poisoning the catalytic reaction, as e.g. in the case of Rh surfaces,<sup>1–3</sup> while recent experiments showed that the high catalytic activity of the Ru(0001) surface with respect to the CO oxidation relates in fact to the existence of RuO<sub>2</sub>(110) oxide patches that form under oxidizing conditions.<sup>4–6</sup> Thus, apparently, unreactive surface oxides are more likely to form on Rh than on Ru surfaces. These findings call for an atomistic understanding of the oxidation of these transition-metal surfaces and of the structure of their oxide surfaces.

There is general agreement that the mechanistic steps leading to oxide formation involve dissociative oxygen chemisorption on the metal surface, lattice penetration of atomic oxygen, and the crystallization and growth of the stoichiometric oxide phases. The sequence of these events may be complex, and rather than successively, they may occur simultaneously, depending on the temperature and pressure. The first of these steps, i.e. the chemisorption of oxygen on Rh single crystal surfaces,

has been the subject of intensive experimental and theoretical research,<sup>7–10</sup> but only few experimental studies have addressed the ensuing formation of sub-surface oxygen,<sup>11–17</sup>. In one of these studies it could recently be shown<sup>16</sup> that exposure of the Rh(111) surface to O<sub>2</sub> at moderately elevated temperatures ( $\sim 470$  K) leads to the formation of sub-surface oxygen species, and there is evidence that at least  $\sim 0.9$  monolayer (ML) of O is adsorbed on the surface before sub-surface sites are occupied. Interestingly, the analysis of the X-ray photoelectron diffraction (XPD) data of the corresponding study suggested that the sub-surface species ( $\sim 0.1$  ML) occupies octahedral sites between the first and second Rh outermost layers, which lie just underneath the fcc on-surface adsorption sites, while the neighboring on-surface oxygen has *switched* from its normal fcc to the hcp sites.

On theory side, *ab initio* studies of O sub-surface species on transition metal surfaces are even more scarce<sup>18–20</sup> and as yet lacking for Rh surfaces. The present theoretical study therefore specifically examines the incorporation of O into the close-packed Rh(111) surface using density-functional theory. Extending preceding work focusing on ordered oxygen phases *on* this surface<sup>9,10</sup> we now discuss the stability of oxygen *below* the surface, and address questions concerning the minimum oxygen coverage at the onset of oxygen penetration (section III.A), the stability of various available sub-surface sites (section III.B), as well as the effect of a continued oxygen incorporation with increasing coverage up to 2.0 ML (section III.C). The present results for sub-surface oxygen on Rh(111) are discussed and compared with corresponding results for the Ru(0001) surface<sup>19,20</sup> as a first step towards the understanding of the elementary steps governing the onset of surface oxide formation. Questions remain as to the nature of the distinct chemical activity of oxidized Ru(0001) and Rh(111) surfaces.

## II. CALCULATIONAL DETAILS

All calculations have been performed using density-functional theory (DFT) and the generalized gradient approximation (GGA) of Perdew *et al.*<sup>21</sup> for the exchange-correlation functional as implemented in the full-potential linear augmented plane wave method (FP-LAPW)<sup>22–24</sup>. The Rh(111) surface is modeled in the supercell approach, employing a 7-layer (111) Rh slab with a vacuum region corresponding to 6 interlayer spacings ( $\approx 13 \text{ \AA}$ ). Oxygen atoms are adsorbed on both sides of the slab. Their positions as well as those of all Rh atoms in the two outermost substrate layers are allowed to relax while the central three layers of the slab are fixed in their calculated bulk positions. In a preceding publication we have detailed the geometrical properties and stability of ordered adlayers of O on Rh(111)<sup>9</sup>. Exactly the same calculational setup is used here, such that the results of our prior study can be used for comparison. Further technical details of the calculations can correspondingly be found in Ref. 9.

We address the stability of O/Rh(111) structures with respect to adsorption of O<sub>2</sub> by calculating the average adsorption energy per O adatom,

$$E_{\text{ad}}(\theta_{\text{tot}}) = E_{\text{b}}(\theta_{\text{tot}}) - D/2, \quad (1)$$

where  $D$  is the dissociation energy of the O<sub>2</sub> molecule and  $E_{\text{b}}(\theta_{\text{tot}})$  the average binding energy per oxygen atom as a function of the total coverage (i.e., on- + sub-surface)  $\theta_{\text{tot}}$ . In turn,  $E_{\text{b}}(\theta_{\text{tot}})$  is defined as

$$E_{\text{b}}(\theta_{\text{tot}}) = -\frac{1}{N_{\text{tot}}} [ E_{\text{O/Rh}(111)}^{\text{slab}}(\theta_{\text{tot}}) - (E_{\text{Rh}(111)}^{\text{slab}} + N_{\text{tot}} E_{\text{O}}^{\text{atom}}) ], \quad (2)$$

where  $N_{\text{tot}}$  is the total number of oxygen atoms in the unit-cell, and  $E_{\text{O/Rh}(111)}^{\text{slab}}$ ,  $E_{\text{Rh}(111)}^{\text{slab}}$ , and  $E_{\text{O}}^{\text{atom}}$  are the total energies of the O/Rh(111) adsorbate system, of the clean Rh(111) surface, and of the free oxygen atom, respectively. A positive value of the average adsorption energy indicates that the dissociative adsorption of O<sub>2</sub> is exothermic. That is, the binding energy per O adatom on Rh(111) is larger than that which the O atoms have in O<sub>2</sub>(gas), i.e.,  $D/2$ . The total energies of the adsorbate system and clean surface are calculated using the same supercell. Details on the calculations of the isolated O atom and the free O<sub>2</sub> molecule are given in Ref. 9.

To test the accuracy of the calculated binding energies,  $E_{\text{b}}(\theta_{\text{tot}})$ , on numerical approximations due to the finite FP-LAPW basis set and the finite slab and vacuum thicknesses in the supercell approach, selected calculations were repeated with higher accuracy. The self-consistent calculations of  $E_{\text{b}}$  were routinely conducted for a 7-layer slab, a 16 Ry plane-wave cutoff in the interstitial region, and a (12 × 12 × 1) Monkhorst-Pack grid for the (1 × 1) unit-cell with 19 k-points in the irreducible wedge<sup>9</sup>. Changing to denser k-meshes up to a (18 × 18 × 1)

grid with 37 k-points in the irreducible wedge resulted in negligible variations of  $E_{\text{b}}$  within  $\sim 10 \text{ meV/O atom}$ . Similarly, extending the Rh(111) slab from 7 to 9 and 11 layers led only to changes in the calculated binding energies up to  $\sim 10 \text{ meV/O atom}$ . The only really notable effect on the computed  $E_{\text{b}}$  is caused by variations of the finite plane-wave cutoff in the interstitial region: Increasing this cutoff from 16 Ry to 24 Ry decreases the binding energies by  $\approx 100 \text{ meV/O atom}$ . Yet, this decrease can be largely attributed to an improved description of both the free O atom and the chemisorbed species and thus affects all structures that contain the same amount of O alike. Consequently, the calculation of relative stabilities of different phases, i.e. the difference between two binding energies, has a significantly smaller error than this variation in the absolute value of  $E_{\text{b}}$ . Combining all these tests, we give a conservative estimate of this latter error of  $\pm 30 \text{ meV/O atom}$ , which in turn does not affect any of the conclusions made in this work.

## III. STABILITY OF SUB-SURFACE O

### A. Minimum coverage for O incorporation

The initial oxidation of the Rh(111) surface proceeds via the dissociative chemisorption of oxygen in the three-fold fcc hollow sites of the basal surface.<sup>7–9</sup> O<sub>2</sub> exposure under UHV conditions leads to two well ordered superstructures, namely a (2 × 2)-O and a (2 × 1)-O phase at coverages of 0.25 ML and 0.5 ML, respectively. The latter coverage was for a long time believed to correspond to a saturated surface.<sup>7</sup> Yet, after theoretical prediction,<sup>8,9</sup> a (1 × 1)-O phase ( $\theta_{\text{tot}} = 1.0 \text{ ML}$ ) could be stabilized experimentally under UHV conditions using atomic O as oxidant, thus demonstrating that the apparent saturation results from a kinetic energy barrier to O<sub>2</sub> dissociation.<sup>17</sup> This barrier can also be overcome by enhanced O<sub>2</sub> dosage at moderately elevated temperatures<sup>13,16,25</sup> or by exposure to more oxidizing carrier gases like e.g. NO<sub>2</sub>.<sup>13,17</sup> In all cases, sub-surface O incorporation or bulk diffusion was reported for higher exposures at temperatures above  $\sim 400 \text{ K}$ , and as already mentioned a recent experimental study brought evidence that at least  $\sim 0.9 \text{ ML}$  of oxygen is adsorbed on the surface, before sub-surface sites become occupied.<sup>16</sup>

To address this initial incorporation theoretically we study the stability and properties of sub-surface oxygen species as function of the total coverage,  $\theta_{\text{tot}}$  ( $0.25 \leq \theta_{\text{tot}} \leq 1.0 \text{ ML}$ ). We employ (2 × 2) unit-cells and calculate the average adsorption energy of fully relaxed structures containing from  $N_{\text{tot}} = 1$  ( $\theta_{\text{tot}} = 0.25 \text{ ML}$ ) up to  $N_{\text{tot}} = 4$  ( $\theta_{\text{tot}} = 1 \text{ ML}$ ) oxygen atoms (see Eq. (2)). The occupation of sub-surface sites will commence, when a structure with one of these O-atoms located below the surface becomes energetically more favorable than the most stable one with all oxygens on the surface at the

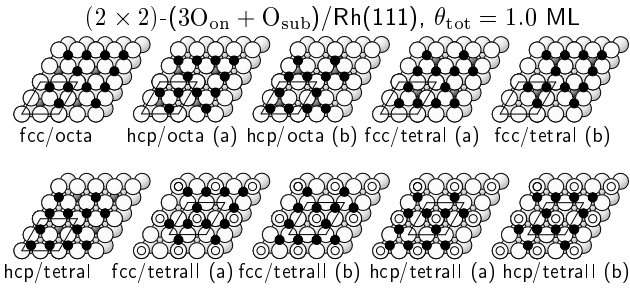


FIG. 1. Top view of all possible on-surface/sub-surface site combinations at  $\theta_{\text{tot}} = 1.0$  ML with one oxygen atom located below the surface (see text for the explanation of the different sites). Rh = big spheres (white = surface layer, grey = 2nd layer), O = small spheres (black = on-surface, grey = sub-surface). Oxygens in tetra-II sites below the first layer Rh atoms are invisible in this plot and are schematically shown as small white circles. Symmetry inequivalent occupation of the same kind of on- and sub-surface sites are denoted with (a) and (b), respectively.

same total coverage. That is, we compare the stability of  $(2 \times 2) - ((N_{\text{tot}} - 1)O_{\text{on}} + O_{\text{sub}})/\text{Rh}(111)$  mixed phases relative to the  $(2 \times 2) - (N_{\text{tot}}O_{\text{on}})/\text{Rh}(111)$  structure with  $O_{\text{on}}$  atoms in fcc hollow sites for  $N_{\text{tot}} = 1, \dots, 4$ .

Between the first and second outermost metal layers, there are three different high-symmetry interstitial sites available for O incorporation. The octahedral site (henceforth octa) lies just underneath the fcc on-surface site, and one tetrahedral site (tetra-I) lies below the hcp on-surface site. A second tetrahedral site (tetra-II) is located directly below a first layer metal atom. Considering both three-fold hollow sites (fcc and hcp) as possible adsorption sites on the surface, leads then to a many-fold of possible structural combinations of how to place the  $N_{\text{tot}}$  oxygen atoms into the unit-cell, in particular as at most coverages several symmetry inequivalent possibilities for the same on- and sub-surface site combination exist.

As will be shown below, the stability of structures involving on- and sub-surface sites becomes only comparable to that of the pure chemisorbed on-surface phase at  $\theta_{\text{tot}} = 1.0$  ML. Thus, only at that coverage we will address the complete set of possible structural combinations, shown in Fig. 1, while at the lower coverages we only exemplify the stability trends by computing three likely combinations that will become relevant at a later stage of our discussion. Namely, these are geometries where on-surface oxygen is in fcc sites and the sub-surface oxygen in either the octa or the tetra-I sites, fcc/octa and fcc/tetra-I respectively. Thirdly, we included the experimentally suggested possibility<sup>16</sup> that oxygen in octahedral sub-surface sites induces a site-switch of the nearby on-surface oxygens from fcc to hcp, viz hcp/octa. The thus resulting set of considered structures is shown in Fig. 2 for  $\theta_{\text{tot}} = 0.5$  ML and  $\theta_{\text{tot}} = 0.75$  ML. At the latter coverage we also tested the possibility of a simul-

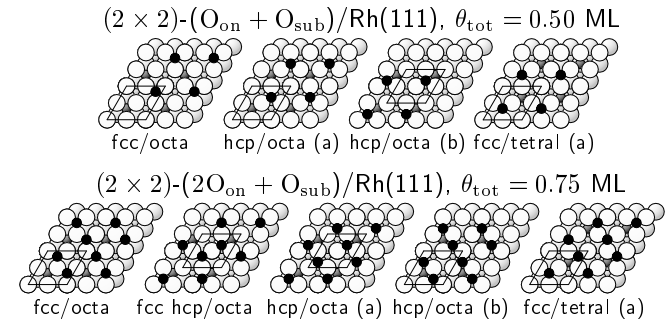


FIG. 2. Top view of selected on-surface/sub-surface site combinations at  $\theta_{\text{tot}} = 0.5$  ML and  $\theta_{\text{tot}} = 0.75$  ML with one oxygen atom located below the surface (see text). Rh = big spheres (white = surface layer, grey = 2nd layer), O = small spheres (black = on-surface, grey = sub-surface).

TABLE I. Average adsorption energies (in eV/O atom) of Rh(111) geometries containing O in on-surface and/or sub-surface sites. The label on/sub indicates the site type (fcc,hcp for on-surface; octa/tetra-I/tetra-II for sub-surface, see text). Calculated values for the most stable on-surface ad-layer with O occupying fcc sites (fcc—) are from Ref. 9. For  $\theta_{\text{tot}} \leq 1.25$  ML, 0.25 ML of O is contained below the surface, for  $\theta_{\text{tot}} = 2.0$  ML, 1.0 ML of O is contained below the surface.

Sites on/sub	$\theta_{\text{tot}}$					
	0.25	0.50	0.75	1.00	1.25	2.00
fcc—	2.24	1.95	1.66	1.40		
—/octa	−1.25					
—/tetraI	−0.78					
fcc/octa		0.36	0.75	0.81	0.69	0.56
fcc hcp/octa		0.68				
hcp/octa (a)		0.81	1.02	0.92	0.81	0.89
hcp/octa (b)		0.34	0.68	0.74		
fcc/tetraI (a)		1.02	1.19	1.07	0.93	1.13
fcc/tetraI (b)				0.74		
hcp/tetraI (a)				0.79		
fcc/tetraII (a)				0.91	0.77	0.83
fcc/tetraII (b)				0.91		
hcp/tetraII (a)				0.80	0.68	0.86
hcp/tetraII (b)				0.85		

taneous occupation of hcp and fcc on-surface sites and octahedral sub-surface sites, leading to the fcc hcp/octa structure. Figs. 1 and 2 also show the considered symmetry inequivalent structures with the same kind of on- and sub-surface sites occupation, e.g. hcp/octa (a) and hcp/octa (b).

The calculated average adsorption energies of all investigated structures are compiled in Table I, while Fig. 3 additionally visualizes the trends for three selected on-surface/sub-surface combinations as described above. Concentrating first on the lowest tested coverage,  $\theta_{\text{tot}} = 0.25$  ML, we find that the occupation of just sub-surface sites without any on-surface oxygen is not even exothermic and by  $\approx 3$  eV/O atom less favorable than adsorp-

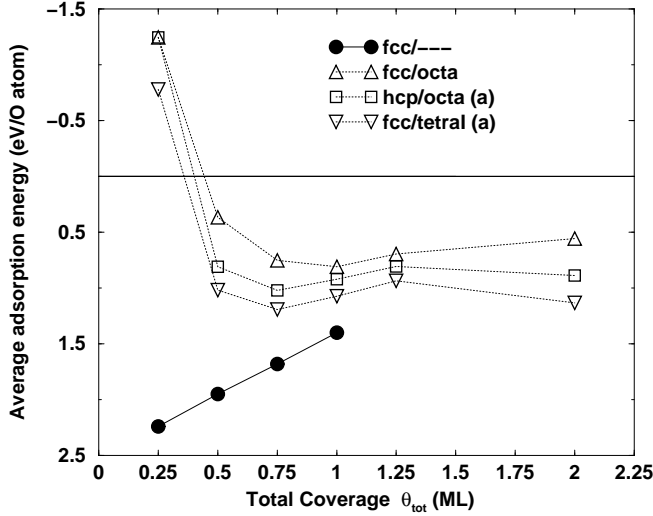


FIG. 3. Average adsorption energies (in eV/O atom) of selected Rh(111) geometries containing O in on-surface and/or sub-surface sites, see text and Table I.

tion into the on-surface fcc hollow sites. We have recently shown that this is generally the case for the closed-packed late 4d transition metal surfaces, which is largely largely due to the significant local expansion of the metal lattice induced by occupation of sub-surface sites.<sup>26</sup> The corresponding cost of distorting the metal lattice and breaking metal bonds renders sub-surface sites initially always less stable than on-surface chemisorption. Yet, upon increasing the on-surface coverage, repulsive interactions between the adsorbates drive the adsorption energy down, cf. Fig. 3, until eventually occupation of sub-surface sites might become more favorable compared to a continued filling of on-surface sites.

Turning therefore to higher coverages up to 1.0 ML, where we continuously increase the number of adsorbed on-surface oxygen atoms per unit cell, we find the average adsorption energies of all mixed structures now to be positive, i.e. they should be able to form. Still, in the whole sub-monolayer regime the values of  $E_{ad}(\theta_{tot})$  for the mixed phases are significantly lower compared to that of the pure on-surface adsorption at the same total coverage, reflecting the above described fact, that the occupation of sub-surface sites is energetically considerably less favorable. Only at  $\theta_{tot} = 1.0$  ML does the adsorption energy of the selected mixed phases approach that of the pure on-surface fcc phase to within  $\approx 0.3$  eV/O atom (cf. Fig. 3). To make sure that no other structural on-surface/sub-surface combination would be even slightly more stable and then eventually more favorable than the pure on-surface phase, we tested all of the possible structures shown in Fig. 1 at this particular coverage. As can be seen from Table I neither of these configurations leads to a more favorable binding than the pure fcc phase. Therefore, O incorporation into the Rh(111) sur-

face can only occur at just about the completion of the full monolayer coverage on the surface, i.e.  $\theta_{tot} \approx 1.0$  ML.

The calculated energy difference of  $\approx 0.3$  eV/O atom between the pure fcc and the mixed phases for coverages  $\theta_{tot} \approx 1.0$  ML indicates that sub-surface O penetration into Rh(111) is an energetically activated process and that a small, but finite concentration of sub-surface oxygen can be expected already at on-surface coverages slightly below 1.0 ML at elevated temperatures. Wider *et al.* have found that extended exposure of the Rh(111) surface to oxygen at 470 K led to the formation of a sub-surface species, though the on-surface coverage remained slightly below 1.0 ML.<sup>16</sup> In comparison, on Ru(0001) we find the energy difference between the pure on-surface and the mixed phases at  $\theta_{tot} = 1.0$  ML to be  $\approx 0.8$  eV/O atom,<sup>27</sup> that is about a factor of three larger than for Rh(111). Correspondingly, oxygen penetration has at the prior surface only been reported to occur *after* the  $(1 \times 1)$ -O phase on the surface has been completed.<sup>29,30</sup>

## B. Site preferences and site-switch

Trying to understand the oxygen site preferences in the various on-surface/sub-surface phases at coverages up to 1.0 ML, we note first that the low stability of a number of structural combinations can be understood in terms of electrostatic repulsion between the oxygens, i.e. whenever the electronegative oxygens come too close to each other. This holds for mixed fcc hcp combinations (cf. Table I), as well as for the less stable of the two symmetry inequivalent possibilities of the same on-surface/sub-surface site combination (rendering e.g. the hcp/octa (b) and fcc/tetra (b) geometries unfavorable, cf. Figs. 1 and 2 and Table I).

Moreover, we find the stability of all other combinations at  $\theta_{tot} = 1.0$  ML to be rather similar, i.e. within  $\approx 0.2$  eV/O atom, cf. Table I. This suggests that at elevated temperatures oxygen incorporation could start initially in all available sites, and that kinetic factors (like penetration barriers) more than energetic factors determine which of the possible metastable sites get populated first in an experiment with controlled oxygen dosage. As noted in the introduction, a recent analysis of XPD data indicated the presence of a sub-surface oxygen species ( $\sim 0.1$  ML) in octahedral sites between the first and second metal layer at an almost oxygen-covered ( $\sim 0.9$  ML) Rh(111) surface after  $10^5$  Langmuir O<sub>2</sub> exposure at 470 K. The analysis of the data yields to the suggested simultaneous occupation of neighboring on-surface hcp sites, which is different from the otherwise preferred fcc sites on Rh(111) before oxygen incorporation.<sup>16</sup>

This intriguing finding is in line with our calculations, which indeed indicate, that *if* sub-surface oxygen was to occupy octahedral sites, then the site-switch combination hcp/octa would be considerably more favorable compared to the fcc/octa combination with the on-surface

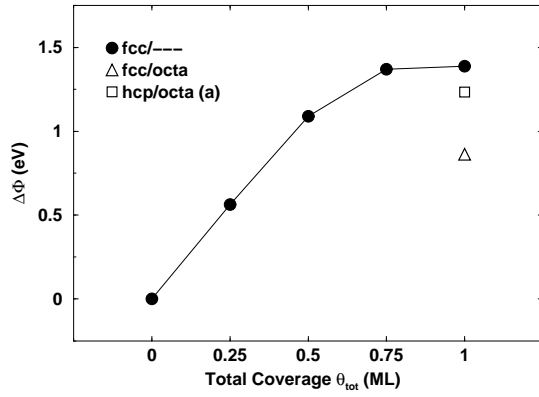


FIG. 4. Calculated work function change for the fcc/octa and hcp/octa (a) structures at  $\theta_{\text{tot}} = 1.0$  ML (see Fig. 1). Calculated values for the most stable adlayers with O occupying only on-surface fcc sites are from Ref. 9.

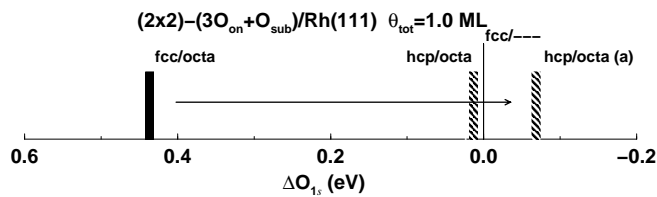


FIG. 5. Calculated initial-state on-surface O 1s core-level shifts for the fcc/octa and hcp/octa (a) phases at  $\theta_{\text{tot}} = 1.0$  relative to the O 1s level for the adatoms of the O-(1×1)/Rh(111) structure at  $\theta_{\text{on}} = 1.0$  ML, with O occupying on-surface fcc sites (fcc/—). The label on/sub indicates the on- and sub-surface adsorption sites, respectively. There are two symmetry inequivalent O adatoms in the hcp/octa phase, which is why two levels are shown for this structure.

oxygens in their normal adsorption sites, cf. Fig. 3.

In seeking for a qualitative explanation for the stability of the hcp on-surface sites upon occupation of octahedral sites, and consistent with the discussion on the preferred fcc site adsorption begun in earlier papers,<sup>9,10</sup> we examine the calculated changes in the work-function,  $\Delta\Phi$ , as well as the difference in O 1s binding energy of on-surface O-atoms,  $\Delta O_{1s}$ , of the mixed fcc/octa and hcp/octa phases at  $\theta_{\text{tot}} = 1.0$  ML relative to the values for the stable (1×1)-O/Rh(111) structure, with O just occupying fcc sites. The calculated  $\Delta\Phi$  and  $\Delta O_{1s}$  values are shown in Figs. 4 and 5, respectively. Initially, the work function rises as a function of the coverage, while O remains in the surface fcc sites; at  $\theta_{\text{tot}} \approx 0.75$  ML it reaches a saturation value. Such an increase in the work-function upon O chemisorption reflects the high electronegativity of the adspecies that results in an induced inward dipole moment, i.e., with the negative charge at the vacuum side of the surface. The saturation at higher coverages is then a consequence of the dipole-dipole interaction giving rise to a depolarization with decreasing

O-O distance.

The initial incorporation of oxygen in the fcc/octa and hcp/octa phases leads to a decrease in the work function compared to the saturation value at 1.0 ML with O just occupying on-surface fcc sites. This decrease is considerably smaller for the hcp/octa structure, cf. Fig. 4; where it should also be noticed that the average bond length,  $O_{\text{on}}\text{-Rh}_1$  and interlayer spacing,  $d_{O_{\text{on}}\text{-Rh}_1}$ , between chemisorbed O and Rh atoms at the surface are practically independent of the occupation of the sites at a given coverage, cf. Tables II and III. Moreover, the calculated initial-state O 1s shifts schematically shown in Fig. 5, indicate that the O 1s levels of adatoms in the hcp/octa geometry are  $\sim 0.5$  eV less bound compared to corresponding levels of oxygen atoms in the fcc/octa geometry. This reflects a larger electrostatic repulsion at the hcp sites, where a somewhat more negatively charged O would be adsorbed, which in turn correlates with the smaller decrease in the work function for the preferred site-switch phase.

On comparing the values of  $\Delta\Phi$  and  $\Delta O_{1s}$  for the hcp/octa and fcc/octa phases with those for the pure fcc adsorption in Figs. 4 and 5 it can thus be suggested that a similarly charged O would sit in hcp sites (rather than in fcc sites) upon octahedral sub-surface occupation compared to the oxygens adsorbed in fcc sites before O penetration. Hence, similarly to the pure on-surface fcc adsorption,<sup>9,10</sup> we suggest that a stronger *ionic* bonding favors the hcp sites in the site-switch phases at the onset of O penetration ( $\theta_{\text{tot}} \approx 1.0$  ML).

Although we can thus rationalize the higher stability of the hcp/octa site-switch phase suggested by Wider *et al.*<sup>16</sup> compared to the fcc/octa phase, we nevertheless stress that the occupation of octahedral sub-surface sites is according to our calculations only of a metastable character, as the fcc/tetra-I structural combination is consistently energetically more favorable over the complete tested coverage range, cf. Fig. 3.

### C. Continued oxidation: island formation and trilayer shift

We investigate the continued oxidation after sub-surface O has been initially incorporated in the coverage region  $1.25 \leq \theta_{\text{tot}} \leq 2.0$  ML by calculating the average adsorption energy at both 1.25 ML ( $\theta_{\text{sub}} = 0.25$  ML) and 2.0 ML ( $\theta_{\text{sub}} = 1.0$  ML) coverages. Again, we find that the site combinations hcp/octa and fcc/tetra-I give the highest adsorption energies, while the occupation of tetra-II sites leads to energetically slightly less favorable phases, cf. Table I. In the following we will restrict our discussion to the two most stable phases, i.e. hcp/octa and fcc/tetra-I.

Tables II ( $\theta_{\text{tot}} = 1.25$  ML) and III ( $\theta_{\text{tot}} = 2.0$  ML) show that the geometrical changes in response to sub-surface penetration of oxygen are significant and it is

TABLE II. Calculated structural parameters in Å for the hcp/octa and fcc/tetra-I phases at  $\theta_{\text{tot}} = 1.25$  ML. O atoms and all Rh atoms in the two outermost layers were allowed to relax. For the interlayer distances, the center of mass of each layer is used. Numbers in parenthesis correspond to bulk values, which were fixed.  $O_{\text{on,sub}}\text{-Rh}_{1,2}$  indicate (averaged) bond lengths to first and second layer Rh atoms, and  $\Delta z_{\text{Rh}_{1,2}}$  and  $\Delta z_{\text{O}_{\text{on}}}$  the magnitude of the buckling of the outermost Rh layers and of the on-surface O adlayer, respectively. The lateral displacements, radially away from the ideal lattice positions, are denoted by  $\Delta r_{\text{Rh}_{1,2}}$ , and  $\Delta r_{\text{O}_{\text{on}}}$ , respectively.

	hcp/octa	fcc/tetra-I
$O_{\text{on}}\text{-Rh}_1$	1.94	1.95
$O_{\text{sub}}\text{-Rh}_1$	2.15	2.00
$O_{\text{sub}}\text{-Rh}_2$	2.21	1.94
$\bar{d}_{O_{\text{on}}\text{-Rh}_1}$	1.14	1.15
$\bar{d}_{12}$	2.79	2.78
$\bar{d}_{23}$	2.30	2.32
$\bar{d}_{34}$	(2.213)	(2.213)
$\Delta z_{\text{Rh}_1}$	0.30	0.23
$\Delta z_{\text{Rh}_2}$	0.26	0.30
$\Delta z_{\text{O}_{\text{on}}}$	0.18	0.18
$\Delta r_{\text{Rh}_1}$	0.06	0.08
$\Delta r_{\text{Rh}_2}$	0.03	0.00
$\Delta r_{\text{O}_{\text{on}}}$	0.07	0.07

TABLE III. Calculated structural parameters in Å for the hcp/octa, fcc/tetra-I, and fcc/tetra-I<sub>fault</sub> phases at  $\theta_{\text{tot}} = 2.0$  ML. O atoms and all Rh atoms in the two outermost layers were allowed to relax. Numbers in parenthesis correspond to bulk values, which were fixed.  $O_{\text{on,sub}}\text{-Rh}_{1,2}$  indicate bond lengths to first and second layer Rh atoms, and  $\bar{d}_{ij}$  interlayer spacings.

	hcp/octa	fcc/tetra-I	fcc/tetra-I <sub>fault</sub>
$O_{\text{on}}\text{-Rh}_1$	1.96	1.97	1.97
$O_{\text{sub}}\text{-Rh}_1$	2.10	2.05	2.06
$O_{\text{sub}}\text{-Rh}_2$	2.51	2.01	2.02
$\bar{d}_{O_{\text{on}}\text{-Rh}_1}$	1.19	1.19	1.19
$\bar{d}_{12}$	3.36	3.34	3.35
$\bar{d}_{23}$	2.14	2.17	2.18
$\bar{d}_{34}$	(2.213)	(2.213)	(2.213)

therefore not accurate to assume that the Rh(111) lattice will remain essentially undisturbed upon the occupation of sub-surface sites. For both hcp/octa and fcc/tetra-I phases at 1.25 ML (0.25 ML below the surface), the mean outermost substrate interlayer spacing,  $\bar{d}_{12}$ , expands by about  $\sim 22\%$ , and  $\sim 26\%$ , relative to the corresponding value for the bulk-terminated surface, respectively (cf. Table II). Prior to the present work, we have calculated an increase of  $\bar{d}_{12}$  from 2.21 Å for the clean surface to 2.37 Å for the  $(1 \times 1)$ -O/Rh(111) structure with oxygens in fcc sites,<sup>9</sup> which means that an additional  $\sim 15 - 19\%$  expansion is induced by the 0.25 ML of sub-surface oxygen.

For the  $(2 \times 2)$ - $(4O_{\text{on}} + O_{\text{sub}})/\text{Rh}(111)$  phases at

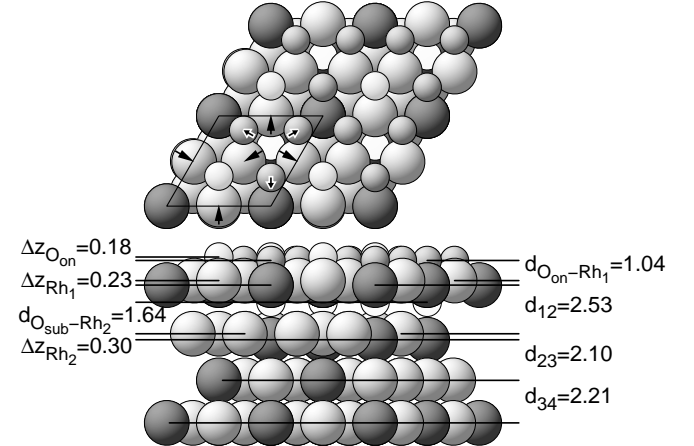


FIG. 6. Top and side view of the fcc/tetra-I geometry at  $\theta_{\text{tot}} = 1.25$  ML. Small and large spheres represent oxygen and Rh atoms respectively, where those lying in the same plane and equivalent under the threefold rotation symmetry have the same color. The arrows indicate the direction of reference for the atomic in-plane displacements  $\Delta r_{\text{Rh}_{1,2}}$ , and  $\Delta r_{\text{O}_{\text{on}}}$  of Table II. Distances are in Å.

1.25 ML, symmetry allows for (in part considerable) buckling of the outermost Rh and on-surface O layers, i.e. quite distinct local contractions and expansions together with lateral shifts (cf. Table II), which can most often be understood as a local expansion of the metal lattice around the occupied sub-surface site.<sup>26</sup> In view of keeping the paper within a limited length, we show only one example. For instance, in the fcc/tetra-I geometry, cf. Fig. 6, the first layer Rh atoms above the occupied sub-surface site, are pulled out of the surface by  $\sim 0.23$  Å, while the neighboring Rh atoms in the second substrate layer are pushed inwards by  $\sim 0.30$  Å. Also, there are local vertical displacements of the O adatoms ( $\sim 0.18$  Å), and considerable lateral shifts radially away from the ideal lattice positions for both substrate and adsorbate atoms.

The expansion of the first Rh layer distance becomes with  $\approx 51\%$  even more pronounced at  $\theta_{\text{tot}} = 2.0$  ML (1 ML O below the surface), cf. Table III. Despite this significant distortion of the metal lattice, we find increased adsorption energies for both the hcp/octa and fcc/tetra-I phases compared to the low sub-surface O coverage at  $\theta_{\text{tot}} = 1.25$  ML, cf. Fig. 3. This reflects an attractive interaction between the sub-surface species, which implies that the latter have a tendency to form *sub-surface islands* (i.e. nucleate) with a local  $(1 \times 1)$  periodicity. For both the hcp/octa and fcc/tetra-I phase, the structure of these islands can be viewed as an  $O_{\text{on}}\text{-Rh}\text{-}O_{\text{sub}}$  trilayer on top of a Rh(111) substrate, cf. Fig. 8. Interestingly, the internal geometry of the strongly bound trilayer is almost identical for both phases, cf. Table III and Fig. 8; it is only the coordination to the underly-

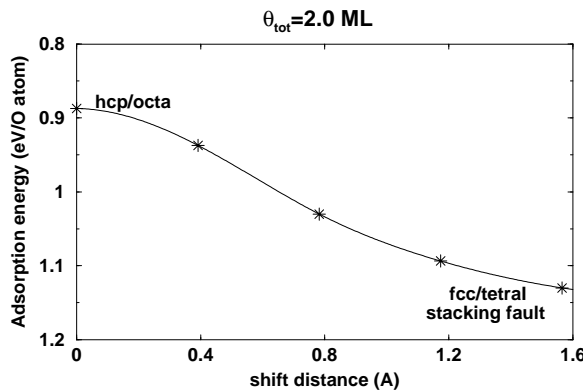


FIG. 7. Calculated average adsorption energy during the registry shift of the  $O_{on}$ -Rh- $O_{sub}$  trilayer along the  $\bar{[2}11]$  direction over the Rh(111) substrate. The initial hcp/octa phase ends in a fcc/tetra-I configuration with a fault in the stacking sequence of the surface Rh layer after shifting the trilayer by  $\frac{a_0}{3}\sqrt{3/2}$  ( $a_0 = 3.83$  Å).

ing substrate which is different in both cases. In fact, we even find that the higher energy hcp/octa configuration is unstable against a registry shift of this whole trilayer along the  $\bar{[2}11]$  direction. The calculated average adsorption energy along this *sliding* of the trilayer over the Rh(111) surface is shown in Fig. 7. We have fully optimized the structures at the calculated points along the *barrierless* displacement, starting from the hcp/octa structure. At the end of the shift by  $\frac{a_0}{3}\sqrt{3/2}$  ( $a_0 = 3.83$  Å, Rh lattice constant<sup>9</sup>), the on-surface oxygen atoms are located in fcc and the sub-surface oxygen atoms in tetra-I sites, but the surface Rh layer inside the trilayer does not continue the fcc lattice stacking, but is now located in a stacking fault position. The calculated structural parameters (interlayer spacings and bond lengths) between these two fcc/tetra-I<sub>fault</sub> and fcc/tetra-I geometries have remained virtually unchanged (cf. Table III), and the average binding energies differ by only  $\sim 3$  meV/O atom, i.e. they are degenerate within our calculational uncertainty, which is plausible as the two structures differ in fact only by a  $60^\circ$  rotation of the trilayer with respect to the underlying substrate. We have similarly compared the geometries and average binding energies of both, fcc/tetraI and fcc/tetraI<sub>fault</sub> structures at 1.25 ML and also found no significant difference; we find a difference of  $\sim 1$  meV/atom in the calculated binding energies.

The reason behind the  $\sim 0.2$  eV/O atom ( $\sim 0.4$  eV/unit cell) preference for the fcc/tetra-I structure compared to the hcp/octa phase can be found when analyzing the coupling of the formed trilayer to the underlying Rh(111) substrate. Whereas we consistently find  $O$ -Rh bondlengths of  $\sim 2.0$  Å for both on- and sub-surface oxygens in the majority of tested structures, the  $O_{sub}$ - $Rh_2$  bondlength of the sub-surface oxygen to the second

layer Rh atom in the hcp/octa phase at  $\theta_{tot} = 2.0$  ML is significantly larger (2.51 Å). This points to a weak coupling of the trilayer to the Rh(111) substrate in this geometry, which can also be seen in the density plots shown in Fig. 8, where the incorporation of sub-surface O in octahedral sites is found to induce only very small changes on the valence charge of the second layer Rh atoms. These changes are considerably larger for the fcc/tetra-I configuration, suggesting that the energetic preference of this structure is primarily due to an improved coupling of the formed trilayer to the underlying substrate.

Hence, even if sub-surface oxygen was initially incorporated into the metastable octahedral sites as suggested by experiment,<sup>16</sup> it would due to this instability transform into the fcc/tetra-I configuration upon continued oxygen penetration into the Rh(111) surface. It is interesting to notice that on the Ru(0001) surface<sup>19,20</sup> a plausible oxidation pathway has been identified, in which after the formation of such trilayers a phase transformation into the rutile  $RuO_2(110)$  structure was obtained for local oxygen coverages exceeding 5 ML. The local formation of such precursing structures via the agglomeration of sub-surface oxygen atoms below the surface that follow the initial oxygen incorporation, could therefore be a more general phenomenon in the oxidation of transition metal surfaces. Once the local oxygen coverage exceeds a critical value, these precursor configurations will then undergo a structural change and actuate the formation of bulk oxide phases. In this respect we notice that already in the preferred fcc/tetra-I configuration the Rh first layer atoms are sixfold coordinated to oxygens and the oxygen atoms in the tetrahedral site fourfold coordinated to metal atoms, i.e. they exhibit identical local coordinations as in the most stable, corundum-structured  $Rh_2O_3$  bulk oxide.

#### IV. SUMMARY

In conclusion we have presented a density-functional theory study addressing the initial penetration of oxygen into the Rh(111) surface. Due to the large local expansion of the metal lattice induced by the occupation of sub-surface sites, O chemisorption on the surface is initially significantly more favorable. In agreement with recent experimental findings, we therefore find oxygen penetration to occur only after the adsorption of *almost* a full monolayer on the surface. A particularly interesting result is that the calculated energy difference of  $\sim 0.3$  eV/atom between the pure on-surface and the mixed on/sub-surface phases at  $\theta_{tot} = 1.0$  ML is about a factor of three smaller than that for Ru(0001). Oxygen penetration has at the Ru surface only been reported to occur *after* the  $(1 \times 1)$ -O phase on the surface has been completed.

The experimentally suggested occupation of octahedral sites in connection with a site-switch of the on-

surface oxygens from fcc to hcp sites is indeed found to be initially possible as a metastable configuration. Increased sub-surface O incorporation will then lead to the agglomeration of sub-surface species. The hcp/octa phase is unstable against a registry shift of the  $O_{on}$ -Rh- $O_{sub}$  outermost layers by which the initial hcp/octa phase ends in a fcc/tetra-I configuration with a fault in the stacking sequence of the surface Rh layer. In this most stable phase, the on- and sub-surface oxygens occupy fcc and tetra-I sites, respectively, and metal atoms are sixfold coordinated to oxygens while the sub-surface oxygen atoms in tetrahedral sites are fourfold coordinated to metal atoms.

The similarities between these results and those of a simultaneous theoretical study of the oxidation of the Ru(0001) surface provide a basis for the interpretation of the role of oxygen incorporation, and nucleation as precursors of the final bulk oxide structure. Addressing the phase transformation to the  $Rh_2O_3$  bulk oxide will thus be of considerable future interest, completing the atomistic pathway of oxide formation at the Rh(111) surface.

## V. ACKNOWLEDGEMENTS

We thank T. Greber, J. Osterwalder, A. Seitsonen, C. Stampfl, F. Illas, and M.E. Grillo for helpful discussions.

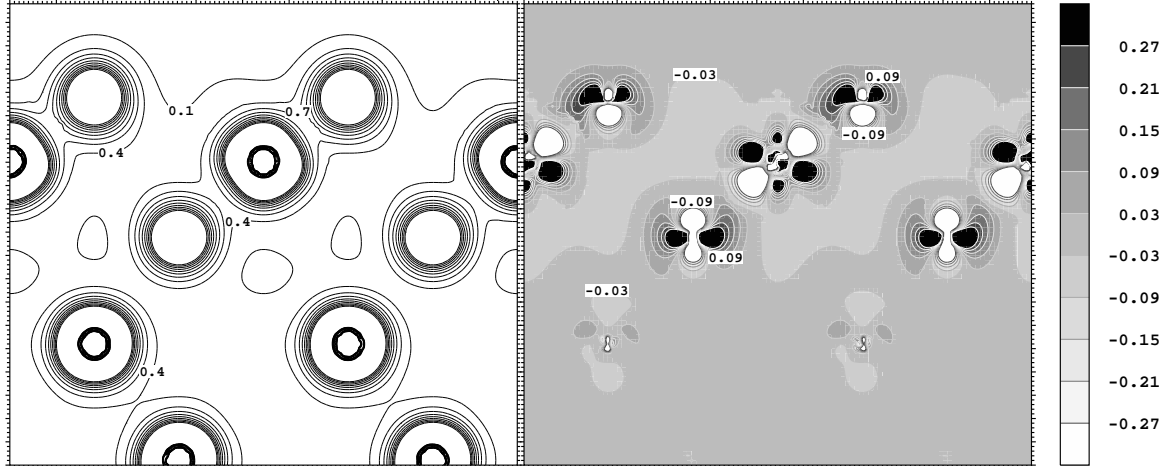
\* Present address: Institut für Chemie, Humboldt Universität zu Berlin, Unter den Linden 6, D-10099 Berlin (Germany).

- <sup>1</sup> S.H. Oh and J.E. Carpenter, *J. Catal.* **80**, 472 (1983).
- <sup>2</sup> G.L. Kellogg, *Phys. Rev. Lett.* **54**, 82 (1985); *Surf. Sci.* **171**, 359 (1986).
- <sup>3</sup> C.H.F. Peden, D.W. Goodman, D.S. Blair, P.J. Berlowitz, G.B. Fisher, and S.H. Oh, *J. Phys. Chem.* **92**, 1563 (1988).
- <sup>4</sup> A. Böttcher, H. Niehus, S. Schwegmann, H. Over, and G. Ertl, *J. Phys. Chem. B* **101**, 11185 (1997).
- <sup>5</sup> H. Over, Y.D. Kim, A.P. Seitsonen, S. Wendt, E. Lundgren, M. Schmid, P. Varga, A. Morgante, and G. Ertl, *Science* **287**, 1474 (2000).
- <sup>6</sup> Y.D. Kim, H. Over, G. Krabbes, and G. Ertl, *Topics in Catal.* **14**, 95 (2001).
- <sup>7</sup> G. Comelli, V.R. Dhanak, M. Kiskinova, K.C. Prince, and R. Rosei, *Surf. Sci. Rep.* **32**, 165 (1998); and references therein.
- <sup>8</sup> D. Loffreda, D. Simon, and P. Sautet, *J. Chem. Phys.* **108**, 6447 (1998).
- <sup>9</sup> M.V. Ganduglia-Pirovano and M. Scheffler, *Phys. Rev. B* **59**, 15533 (1999).
- <sup>10</sup> M.V. Ganduglia-Pirovano, M. Scheffler, A. Baraldi, S. Lizzit, G. Comelli, G. Paolucci, and R. Rosei, *Phys. Rev. B* **63**, 205415 (2001).
- <sup>11</sup> P. A. Thiel, J. T. Yates Jr., and W. H. Weinberg, *Surf. Sci.* **82**, 22 (1979).

- <sup>12</sup> M. Rebholz, R. Prins, and N. Kruse, *Surf. Sci.* **269/270**, 293 (1992).
- <sup>13</sup> K.A. Peterlinz and S.J. Sibener, *J. Phys. Chem.* **99**, 2817 (1995).
- <sup>14</sup> K. D. Gibson, J. I. Colonell, and S. J. Sibener, *Surf. Sci.* **343**, L1155 (1995).
- <sup>15</sup> N. M. H. Janssen, A. Schaak, B. E. Nieuwenhuys, and R. Imbihl, *Surf. Sci.* **364**, L555 (1996).
- <sup>16</sup> J. Wider, T. Greber, E. Wetli, T.J. Kreutz, P. Schwaller, and J. Osterwalder, *Surf. Sci.* **417**, 301 (1998); *ibid.* **432**, 170 (1999).
- <sup>17</sup> K.D. Gibson, M. Viste, E.C. Sanchez, and S.J. Sibener, *J. Chem. Phys.* **110**, 2757 (1999); *ibid.* **112**, 2470 (2000).
- <sup>18</sup> A. Kiejna and B. I. Lundqvist, *Phys. Rev. B* **63**, 085405 (2001); *ibid. Phys. Rev. B* **64**, 049901 (2001).
- <sup>19</sup> K. Reuter, C. Stampfl, M.V. Ganduglia-Pirovano, and M. Scheffler, *Chem. Phys. Lett.* **352**, 311 (2002).
- <sup>20</sup> K. Reuter, M.V. Ganduglia-Pirovano, C. Stampfl, and M. Scheffler, *Phys. Rev. B* (*in press*).
- <sup>21</sup> J.P. Perdew, J.A. Chevary, S.H. Vosko, K.A. Jackson, M.R. Pederson, D.J. Singh, and C. Fiolhais, *Phys. Rev. B* **46**, 6671 (1992).
- <sup>22</sup> P. Blaha, K. Schwarz, and J. Luitz, **WIEN97, A Full Potential Linearized Augmented Plane Wave Package for Calculating Crystal Properties**, Karlheinz Schwarz, Techn. Universität Wien, Austria, (1999). ISBN 3-9501031-0-4.
- <sup>23</sup> B. Kohler, S. Wilke, M. Scheffler, R. Kouba, and C. Ambrosch-Draxl, *Comp. Phys. Commun.* **94**, 31 (1996).
- <sup>24</sup> M. Petersen, F. Wagner, L. Hufnagel, M. Scheffler, P. Blaha, and K. Schwarz, *Comp. Phys. Commun.* **126**, 294 (2000).
- <sup>25</sup> D.G. Castner and G.A. Somorjai, *Appl. Surf. Sci.* **6**, 29 (1980).
- <sup>26</sup> M. Todorova, W.X. Li, M.V. Ganduglia-Pirovano, C. Stampfl, K. Reuter, and M. Scheffler, *Phys. Rev. Lett.* (*submitted*).
- <sup>27</sup> The value of  $\approx 0.8$  eV/O atom was calculated by comparing the average adsorption energy of  $(2 \times 2)$ - $(3O_{on} + O_{sub})/Ru(0001)$  ordered structures with that of a full adlayer on the surface [ $(1 \times 1)$ -O/Ru(0001), with O on hcp sites]. The coadsorbate structures considered on Ru(0001) are analogous to the fcc/tetraI (a)-(b), and the hcp/oct (a)-(b) of Fig. 1. Calculations were performed within the same computational scheme as employed in the present study, modelling the metal surface by a six layer slab. Details of the used FP-LAPW basis set are those described in Refs. 20,28.
- <sup>28</sup> S. Lizzit, A. Baraldi, A. Groso, K. Reuter, M. V. Ganduglia-Pirovano, C. Stampfl, M. Scheffler, M. Stichler, C. Keller, W. Wurth, and D. Menzel, *Phys. Rev. B* **63**, 205419 (2001).
- <sup>29</sup> C. Stampfl, S. Schwegmann, H. Over, M. Scheffler, and G. Ertl, *Phys. Rev. Lett.* **77**, 3371 (1996).
- <sup>30</sup> A. Böttcher and H. Niehus, *J. Chem. Phys.* **110**, 3186 (1999).

$(2 \times 2) - (4O_{on} + 4O_{sub})/Rh(111)$   $\theta_{tot} = 2.0$  ML

hcp/octa



fcc/tetral

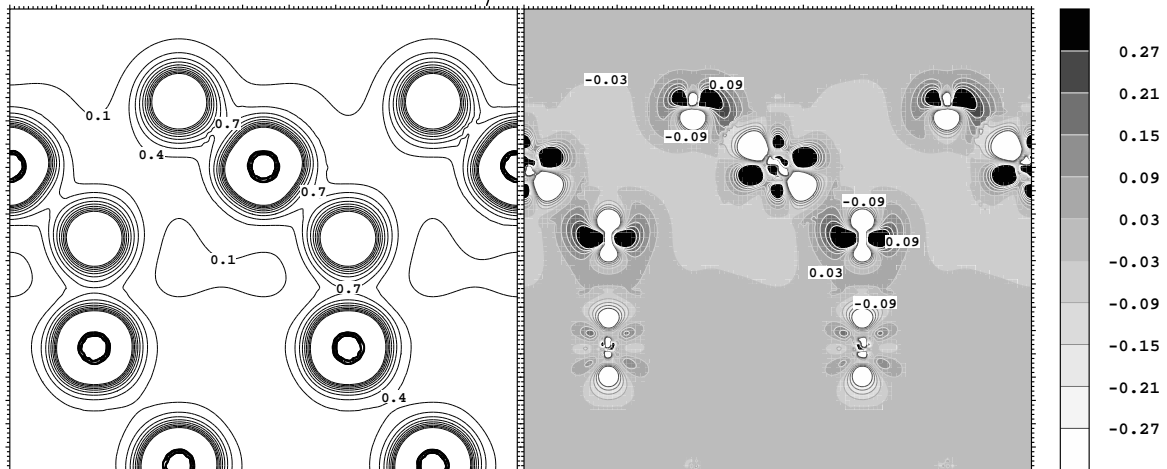


FIG. 8. Left: Contour plots of constant electron density in a  $\bar{[2}11]$  plane perpendicular to the (111) surface of  $(2 \times 2) - (4O_{on} + 4O_{sub})/Rh(111)$  structures with oxygens in hcp/octa (top) and fcc/tetra-I (bottom) sites. Right: Plot of the difference charge density of the same plane, i.e. where the charge density of the clean Rh(111) surface (with distances between Rh atoms as in the chemisorbed system) and those of the isolated oxygens have been subtracted from the electron density shown to the left. The distance between contours is  $0.3 e/\text{\AA}^3$  (left) and  $0.06 e/\text{\AA}^3$  (right). In both cases, the improved bonding of the trilayer to the underlying Rh(111) substrate can be seen as an increase in the bonding charge density to the second layer Rh atoms.